

**Lattice mean-field method for stationary polymer diffusion**

S. M. Scheinhardt-Engels,\* F. A. M. Leermakers, and G. J. Fleer

*Laboratory of Physical Chemistry and Colloid Science, Wageningen University, Dreijenplein 6, 6703 HB Wageningen, The Netherlands*

(Received 15 October 2002; published 15 July 2003)

We present a method to study mean-field stationary diffusion (MFSD) in polymer systems. When gradients in chemical potentials vanish, our method reduces to the Scheutjens-Fleer self-consistent field (SF-SCF) method for inhomogeneous polymer systems in equilibrium. To illustrate the concept of our MFSD method, we studied stationary diffusion between two different bulk mixtures, containing, for simplicity, noninteracting homopolymers. Four alternatives for the diffusion equation are implemented. These alternatives are based on two different theories for polymer diffusion (the slow- and fast-mode theories) and on two different ways to evaluate the driving forces for diffusion, one of which is in the spirit of the SF-SCF method. The diffusion profiles are primarily determined by the diffusion theory and they are less sensitive to the evaluation of the driving forces. The numerical stationary state results are in excellent agreement with analytical results, in spite of a minor inconsistency at the system boundaries in the numerical method. Our extension of the equilibrium SF method might be useful for the study of fluxes, steady state profiles and chain conformations in membranes (e.g., during drug delivery), and for many other systems for which simulation techniques are too time consuming.

DOI: 10.1103/PhysRevE.68.011802

PACS number(s): 36.20.-r, 66.10.Cb, 47.11.+j, 05.50.+q

**I. INTRODUCTION**

Polymeric interfaces [1], brushes [2], vesicles [3], and individual polyelectrolytes [4] are examples of systems that can be studied successfully by using the Scheutjens-Fleer self-consistent-field (SF-SCF) method [5,6]. This is a numerical mean-field approach, yielding the (inhomogeneous) volume fractions and all thermodynamic properties for the systems *at equilibrium*. However, the *stationary states* of such systems are of great interest in the context of, for example, drug delivery over membranes, diffusion-controlled reactions at catalyst surfaces or diffusion over technical membranes in separation processes. To study such stationary polymer systems, the SF-SCF method needs to be extended by dynamic equations and new boundary conditions. We implemented such an extension for a relatively simple system, namely, the diffusion layer between two different homogeneous mixtures, consisting of homopolymer blends or homopolymer solutions. Such a system is of interest for polymer diffusion at long time scales. Our method to study the stationary polymer diffusion will be referred to as the mean-field stationary diffusion (MFSD) method. Equilibrium SCF methods have been extended to dynamic SCF methods before, but our focus is different. The objective of previous extensions was to follow the evolution of a system towards its equilibrium or any other stationary state. Specifically, it was attempted by means of a dynamic version of the SF-SCF method to follow polymer adsorption processes from near-equilibrium towards equilibrium [7]. Two other methods (an off-lattice dynamic self-consistent-field method [8] and a dynamic density functional theory [9,10]) were applied to study the process of spinodal decomposition in (co-)polymer blends. The dynamic density functional theory was also used to investigate the structure development of polymer adsorp-

tion layers [11] and, more relevant to our study, the interface formation by polymer interdiffusion [12]. Here we will not consider the evolution towards a stationary state but focus on a well-defined time-independent solution, that is, the (exact) stationary state itself. Obviously, this restriction allows more efficient computation algorithms than the dynamic methods that construct dynamical trajectories. Such methods need an additional noise term in the diffusion equations to allow the system to escape from local minima of the free energy profile [8,10]. The density functional theory has recently also been applied to study just the stationary state, but only in the application to simple fluids [13]. As in the above-mentioned dynamic mean-field theories, we do not consider hydrodynamic interactions. At present, particle-based simulation methods, which are rather time consuming, are best suited to study polymer dynamics in the presence of hydrodynamic effects [14]. Our method cannot deal with these hydrodynamic effects in full detail. However, the average effect of chain entanglements may easily be modeled in the MFSD method by introducing effective mobility parameters.

Polymer diffusion has attracted attention due to its occurrence and importance in many processes, such as phase separation and spinodal decomposition, bio-adhesion, stabilization of polymer/polymer interfaces by copolymers, diffusion-controlled reactions, etc. A large activity in theoretical work [15–25] accompanies the experimental studies [26–32] in this field. The theoretical interest arises from the fundamental problem of linking together thermodynamic and kinetic properties of polymer mixtures. The mutual (or inter-)diffusion coefficient, governing the relaxation of concentration gradients by the mechanism of particle exchange, is usually written as a product of a thermodynamic factor  $\mathcal{T}$  and a kinetic factor  $\mathcal{K}$  [15,16,20,23]. Interdiffusion is a collective process, in contrast to tracer or self-diffusion, which concerns single-chain motions. The driving force for the latter is entropy and the mechanism may be described by the Rouse

\*Electronic address: Sonja.Engels@wur.nl

[33] or reptation [34,35] models. The tracer and self-diffusion coefficients are relatively easily obtained from experiments. A major topic of research has been on the question whether the mutual diffusion coefficient can be written in terms of these tracer diffusion coefficients.

Two (conflicting) attempts to find such a relation for binary systems are the slow-mode theory [15] and the fast-mode theory [16,17]. The mutual diffusion coefficients of both theories have the same thermodynamic factor  $\mathcal{T}$ . However, the fast-mode theory predicts the kinetic factor  $\mathcal{K}$  to depend linearly on the tracer diffusion coefficients, whereas according to the slow-mode theory the inverse of the kinetic factor depends linearly on the inverse of the tracer diffusion coefficients. This discrepancy originates from different assumptions concerning the compressibility of the system or, according to a statistical mechanical approach [19], from different assumptions concerning the friction coefficient between the diffusing components. Some experiments are in favor of the slow-mode theory [21,36], but most experiments seem to be described best by the fast-mode theory [27,30,31,37]. However, it is stated in Ref. [24] that the initial concentration relaxations as measured in the experiments may incorrectly *appear* to be fast mode. Shearmur *et al.* [28,29] suggest that the preference for the fast-mode theory may arise from the fact that experiments are usually performed at temperatures far from the glass transition temperature. Their experiments follow slow-mode behavior at low temperatures and fast-mode behavior at high temperatures. They find a transition region in which neither of these theories applies. A few theories for polymer diffusion have been derived which reproduce the slow- and fast-mode results in some limiting cases. For example, a hybrid “fast-slow” theory was proposed [18]. According to this theory, there exists a critical diffusion distance beyond which the diffusion changes from fast-mode behavior to slow-mode behavior. Jilge *et al.* [20] adopted an approach, which is similar to the fast-mode theory, but they took into account cross coefficients and vacancy concentrations. The slow- and fast-mode results were obtained by making some approximations, but they concluded that, in general, no simple relation exists between the mutual diffusion and the tracer diffusions. More recently, Akcasu, Nägele, and Klein (ANK) presented a statistical mechanical theory that reduces to the slow- and fast-mode models in the limits of, respectively, vanishing or large vacancy concentrations [23,38]. According to the ANK theory, a cooperative diffusion coefficient is involved in the mutual diffusion. The conclusions of this theory and of Shearmur’s observations [29] are opposite to the predictions of Brereton [21] who constructed a linear combination of the slow- and fast-mode theory.

The above résumé illustrates that the behavior of collectively diffusing polymers is still controversial. We do not aim at resolving this controversy. Instead, we show that it is possible to study stationary diffusion efficiently by our extension to the SF-SCF method. In principle, the flux equations that are employed in our MFSD method can be chosen to conform any of the proposed theories in the literature. For our flux equations, we have chosen the most widely used limiting cases: the slow- and fast-mode theories. The advantage

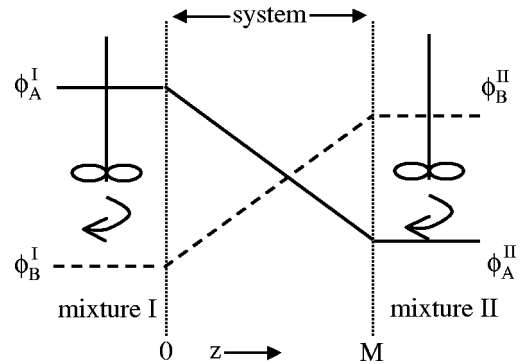


FIG. 1. Schematic representation of the system of study. Stationary diffusion occurs between two infinitely large bulk mixtures I and II which are ideally stirred, so that the volume fractions in these mixtures are constant. The volume fraction profiles in the system are drawn as straight lines for simplicity.

of this choice is that the continuity equation can be solved analytically for some simple stationary systems. This allows the verification of the MFSD results. Using the MFSD method to solve the equation of continuity, the driving forces can be calculated exactly and the detailed conformations of chains may be studied. Moreover, MFSD calculations are much cheaper than simulations: it takes only minutes to calculate all characteristics of the desired stationary state. The equilibrium SF-SCF method, which is our starting point, has proven its applicability to many situations in which stationary diffusion may be of interest.

This paper is organized as follows. In the theoretical section (Sec. II) we first describe the diffusion system for which we developed the MFSD method. We then outline the MFSD method itself, thereby showing that it is based upon the ideas of the equilibrium SF-SCF method. Attention is paid to the evaluation of the driving forces for diffusion (segment chemical potential gradients) and to the slow- and fast-mode flux expressions. These flux expressions were originally derived for binary mixtures, but they can easily be generalized to multicomponent systems, as we will demonstrate. We use each flux equation in combination with two ways to calculate the driving forces for diffusion, so that we obtain four models for the polymer diffusion. Section III presents the results of applying the MFSD method to these four diffusion models. We aim at showing the concept of the MFSD method. Therefore, we focus on the stationary diffusion profiles, although much more information may be extracted from the MFSD calculations. In Sec. IV we discuss the performance of the MFSD method by comparing its numerical results with analytical results. Moreover, we discuss the general characteristics of the diffusion profiles in athermal binary and multicomponent systems. Section V summarizes our conclusions.

## II. THEORY

### A. System

We developed the MFSD method for a setup, as shown in Fig. 1. Two homogeneous polymer bulk mixtures, denoted I and II, are connected by a diffusion layer. Each of these two

mixtures has its own composition, expressed in terms of volume fractions as  $\phi_A^I, \phi_B^I, \phi_C^I, \dots$ , and  $\phi_A^{II}, \phi_B^{II}, \phi_C^{II}, \dots$ , respectively. Here  $A, B, C, \dots$ , denote the various homopolymers or solvent molecules in the mixtures. It is assumed that both mixtures are infinitely large and continuously stirred. As a result, these solutions or blends can be regarded as two bulk mixtures with invariant compositions. The actual system of interest is the layer between the two bulk mixtures. At each side of the system the volume fractions are known (namely,  $\phi^I$  and  $\phi^{II}$ ) and our MFSD method calculates the volume-fraction profiles in the diffusion layer for the stationary state, resulting from diffusion of the molecules for which  $\mu^I \neq \mu^{II}$ , where the  $\mu$ 's are the chemical potentials. The stationary state is defined by constant material fluxes, ensuring that there is no accumulation of any component within the system:  $J_A(z, t) = \text{constant}$  in  $z$  and  $t$ . Note that the flux is taken to be dependent on the  $z$  coordinate only, where  $z$  is the direction along the diffusion layer. This means that we use a one-dimensional (1D) mean-field method. The diffusion layer is divided in  $M$  lattice layers perpendicular to  $z$ .

At present, we model only homodisperse homopolymers and solvent molecules (regarded as monomers). A system containing copolymers would require a different approach for the boundary conditions. In the results Sec. III only athermal systems will be considered (i.e., all Flory-Huggins parameters  $\chi$  are). In the present theoretical section, we treat the more general case of systems with interactions.

The calculation of the volume fractions (as functions of segment potentials) is dictated by the stationarity condition. The derivation of the desired equation follows the steps from equilibrium SF-SCF theory, but requires a different Lagrange parameter, as shown in Sec. II B. From the theory outlined in that section, we find an expression for the exact segment chemical potential (Sec. II C), which is inserted into the Smoluchowski equation that describes the diffusion of the polymers in an external potential field (Sec. II D). In our case the external potential comprises contributions from segmental interactions and from the incompressibility constraint. The slow-mode and fast-mode theories are different in the way they deal with the incompressibility constraint. They thus yield different expressions for the segmental fluxes. In Sec. II D these fluxes are derived in terms of chemical potential gradients and concentration-independent diffusion coefficients. In Sec. II H, we rewrite them in terms of concentration gradients and concentration-dependent diffusion coefficients for analytical purposes.

### B. The MFSD method

The equilibrium SF-SCF method [39] provides an easy way to calculate volume fraction profiles for inhomogeneous (multicomponent) systems at equilibrium. The polymers in these systems are described as chains of segments (comparable with Kuhn segments). Since we are considering only homodisperse homopolymers, the number of components is equal to the number of segment types and we can refer to a component just by referring to its constituent segment type  $A, B, C, \dots$ . The chain length of homopolymer  $A$  is given by  $N_A$ , i.e., the number of segments of type  $A$  that form the

whole chain. The conformation of a chain is given by the position of each segment. The SF-SCF method optimizes the partition function  $Q$  for a lattice in which each lattice site is occupied by a polymer segment, a monomer or a vacancy. Consider a 1D system described by  $M$  lattice layers ( $z = 1, \dots, M$ ). Then the optimization of the partition function must be performed under  $M$  constraints:

$$\sum_A \phi_A(z) = 1 \quad \forall z \in [1, M], \quad (1)$$

where the sum over  $A$  denotes summation over all components (or over all segments, which is identical in our system of homodisperse homopolymers). Therefore,  $M$  Lagrange parameters  $\alpha(z)$  are introduced in the equilibrium SF-SCF method, which are interpreted as the space-filling potentials. The requirements for equilibrium then become

$$\frac{\partial}{\partial n_j^c} \left[ \ln Q + \sum_z \alpha(z) \left\{ \sum_A \phi_A - 1 \right\} \right] = 0 \quad \forall n_j^c, \quad (2a)$$

$$\frac{\partial}{\partial \alpha(z)} \left[ \ln Q + \sum_z \alpha(z) \left\{ \sum_A \phi_A - 1 \right\} \right] = 0 \quad \forall z \in [1, M]. \quad (2b)$$

The parameter  $n_j^c$  denotes the number of molecules  $j$  in a specified conformation  $c$ . Obviously, Eq. (2b) ensures the constraint of incompressibility to be fulfilled. Equation. (2a) dictates the way in which the volume fractions  $\phi$  must be calculated from given segment potentials to obtain the conformation distribution with minimal free energy. The volume fractions depend on the potentials, but the potentials are also dependent on the volume fractions, for example, due to unfavorable segment-segment contacts. The equilibrium SF-SCF algorithm is an iterative procedure that leads to a fixed point for which the potentials are consistent with the volume fractions that obey the constraints.

In the MFSD method, the volume fractions are calculated similarly. Thus, the volume fractions in the stationary state correspond to that conformation distribution of all molecules for which the free energy is minimal. We apply the SF-SCF free energy functional, which is valid for equilibrium systems. It is common to use equilibrium functionals for off-equilibria, since usually the true free energy functionals are unknown [40]. We do not consider this as a serious approximation, since we are only interested in the steady state and not in the evolution towards the steady state. We thus do not need to include a noise term as is usually done in the density functional theory. There is a small difference between the calculation of  $\phi$  in SF-SCF and that in MFSD. This is due to the extended set of constraints for the stationary state. For the stationary state, we have the constraints

$$\phi_A(0) = \phi_A^I \quad \forall A, \quad (3a)$$

$$\phi_A(M+1) = \phi_A^{II} \quad \forall A, \quad (3b)$$

$$\sum_A \phi_A(z) = 1 \quad \forall z \in [1, M], \quad (3c)$$

$$\frac{\partial \phi_A(z)}{\partial t} = 0 \quad \forall A, z \in [1, M]. \quad (3d)$$

The first constraints [given by Eqs. (3a) and (3b)] are treated separately by the boundary conditions (see Sec. II G). The next  $M$  constraints [Eq. (3c)] are obeyed by additional stop criteria for the iterations that must lead to the consistency between the potentials and the volume fractions (see Sec. II F). The number of constraints left is  $M^*$  (number of segment types) [Eq. (3d)]. We assume that there exists only one volume fraction profile, which obeys all constraints and has the minimal free energy. If this profile is given by  $\phi_A^{\text{stat}}(z)$ , the constraints in Eq. (3d) may be summarized by

$$\phi_A(z) = \phi_A^{\text{stat}}(z) \quad \forall A, z \in [1, M]. \quad (4)$$

The requirements for the stationary state become

$$\frac{\partial}{\partial n_j^c} \left[ \ln Q + \sum_{A,z} \alpha_A(z) \{ \phi_A^{\text{stat}}(z) - \phi_A(z) \} \right] = 0 \quad \forall n_j^c, \quad (5a)$$

$$\frac{\partial}{\partial \alpha_A(z)} \left[ \ln Q + \sum_{A,z} \alpha_A(z) \{ \phi_A^{\text{stat}}(z) - \phi_A(z) \} \right] = 0 \quad \forall A, z \in [1, M]. \quad (5b)$$

We thus have the correct number of Lagrange parameters if we take  $\alpha(z)$  to be dependent on the segment type. The volume fractions in the stationary state are calculated in the same way as in equilibrium, but now by introducing the new space filling potentials  $\alpha_A(z)$  in the segment potentials  $u_A(z)$ . Following Ref. [41], we have

$$\frac{u_A(z)}{kT} = \alpha_A(z) + \sum_B \chi_{AB} \langle \phi_B(z) \rangle + \frac{u_A^{\text{ref}}}{kT}, \quad (6)$$

where the reference potential  $u_A^{\text{ref}}$  can be chosen arbitrarily. [In the case of copolymers all constraints should be written in terms of  $\phi_{Ai}$ , the volume fraction of segments  $A$  which are part of molecule  $i$ . The Lagrange parameters  $\alpha$  (and therefore also the segment potentials  $u$ ) would be dependent both on molecule type and on segment type. In SF-SCF, the segment potentials are always independent of the types of molecules [41]]. The angular brackets denote the contact-weighted average over three layers  $z-1$ ,  $z$ ,  $z+1$ :

$$\langle \phi_B(z) \rangle = \lambda_{-1} \phi_B(z-1) + \lambda_0 \phi_B(z) + \lambda_{+1} \phi_B(z+1). \quad (7)$$

$\lambda$ 's account for the number of contacts between lattice, sites. For a simple cubic lattice  $\lambda_0 = 4/6$  and  $\lambda_{-1} = \lambda_{+1} = 1/6$ . The potentials  $u_A(z)$  determine the Boltzmann-weighting factors  $G_A(z)$ ,  $G_A(z, s|1)$ , and  $G_A(z, s|N_A)$ :

$$G_A(z) = \exp \left\{ \frac{-u_A(z)}{kT} \right\}, \quad (8a)$$

$$G_A(z, s|1) = G_A(z) \langle G_A(z, s-1|1) \rangle, \quad (8b)$$

$$G_A(z, s|N_A) = G_A(z) \langle G_A(z, s+1|N_A) \rangle. \quad (8c)$$

The quantity  $G_A(z, s|1)$  is the weighting factor for the last segment of a chain of length  $s$ , where segment  $s$  is in layer  $z$ , while segment 1 may be anywhere in the system. Similarly,  $G_A(z, s|N_A)$  is the weighting factor for the first segment of a chain of length  $N_A - s + 1$ , where the first segment ( $s$ ) is in layer  $z$ , while the last segment ( $N_A$ ) may be anywhere. The starting conditions for Eqs. (8b) and (8c) are  $G_A(z, 1|1) = G_A(z)$  and  $G_A(z, N_A|N_A) = G_A(z)$ . In terms of these weighting factors, the volume fraction of segment  $s$  of component  $A$  in layer  $z$  must be calculated according to Eqs. (5a) and (5b) by

$$\phi_A(s, z) = C_A \frac{G_A(z, s|1) G_A(z, s|N_A)}{G_A(z)}, \quad (9)$$

where  $C_A$  is a normalization constant. Reference [41] considers different ways to normalize volume fractions in equilibrium SF-SCF, but the MFSD results are not influenced by the choice of  $C_A$ , since the driving forces for diffusion are gradients that are independent of the constant  $C_A$ . Equation (9) can also be derived intuitively: the volume fraction of segment  $s$  in layer  $z$  is given by the normalized weighting factor for the probability to find  $s$  in  $z$ , while both the first and the last segment of the chain may be anywhere in the lattice. The chain can be considered as consisting of two parts, one running from segments 1 to  $s$  and the other from segment  $s$  to  $N_A$ . The desired weighting factor can thus be decomposed into the end-segment weighting factors for these parts [as in the numerator in Eq. (9)]. The denominator of Eq. (9) corrects for the double counting the effect of the potential field felt by segment  $s$  that connects the two chain parts.

### C. Segment chemical potentials

Since the partition function is known in the SF-SCF and MFSD calculations, all desired thermodynamical quantities may be calculated. We are interested in the diffusion of segments due to imposed gradients in the chemical potentials. The segment chemical potential is defined as the derivative of the free energy with respect to the volume fraction of the segment under consideration. The resulting expression is [7]

$$\begin{aligned} \frac{\mu_A^{\text{SCF}}(z)}{kT} &= \frac{\partial(F - F^{\text{ref}})/kT}{\partial \phi_A(z)} = - \frac{\partial(\ln Q - \ln Q^{\text{ref}})}{\partial \phi_A(z)} \\ &= \frac{\ln N_A C_A}{N_A} - \frac{u_A(z)}{kT} + \sum_B \chi_{AB} \langle \phi_B(z) \rangle \\ &\quad - \frac{1}{2} \sum_B \chi_{AB} \phi_B^{\text{ref}}, \end{aligned} \quad (10)$$

so that the gradient of the segment chemical potential is easily calculated by

$$\nabla \frac{\mu_A^{\text{SCF}}(z)}{kT} = -\nabla \frac{u_A(z)}{kT} + \nabla \sum_B \chi_{AB} \langle \phi_B(z) \rangle = -\nabla \alpha_A(z). \quad (11)$$

By these expressions we take into account the inhomogeneity of the system. In the following, we will therefore refer to these potentials as the ‘‘exact segment chemical potentials,’’ or the ‘‘SCF potentials.’’ Brochard [15] and Kramer [16], on the contrary, approximate the segment chemical potentials by  $\mu_A^{\text{app}} = \mu_A^{\text{chain}}/N_A$ , where  $N$  is the chain length and where  $\mu^{\text{chain}}$  is obtained from the Flory-Huggins lattice theory [42]. This definition for the segment chemical potential is less accurate when the compositions change significantly within the region where the chain finds itself. Generalizing Brochard’s and Kramer’s approach for binary systems to multi-component homopolymer systems, we obtain for the segment chemical potential of segment type  $A$ :

$$\frac{\mu_A^{\text{app}}}{kT} = \frac{\ln \phi_A}{N_A} + \frac{1}{N_A} - \sum_B \frac{\phi_B}{N_B} - \frac{1}{2} \sum_{BC} (\phi_B - \delta_{AB}) \times \chi_{BC} (\phi_C - \delta_{AC}). \quad (12)$$

Here,  $\delta_{AB}$  ( $\delta_{AC}$ ) is the Kronecker delta, which is unity for  $A=B$  ( $A=C$ ) and 0 otherwise. The independent variables of the segment chemical potentials are given by the volume fractions of all components except one that we denote as component  $X$ . The volume fraction  $\phi_X$  is of course equal to  $1 - \sum_{B \neq X} \phi_B$ . In order to write the flux in terms of  $\phi$  gradients instead of  $\mu$  gradients (for analytical purposes) we take the total differential of the approximate segment chemical potential:

$$\begin{aligned} \nabla \frac{\mu_A^{\text{app}}}{kT} &= \frac{1}{kT} \sum_{B \neq X} \left( \frac{\partial \mu_A^{\text{app}}}{\partial \phi_B} \right)_{\phi_{C \neq B, X}} \nabla \phi_B \\ &= \sum_B \left( \frac{\delta_{AB}}{\phi_A N_A} - \frac{1}{N_B} + \chi_{AB} - \sum_C \phi_C \chi_{BC} \right) \nabla \phi_B. \end{aligned} \quad (13)$$

The gradients of the approximate and exact potentials are indistinguishable if only monomers are present or if the system is homogeneous.

#### D. Flux equations

One of the constraint sets for MFSD, namely, Eq. (3d), can easily be translated in terms of material fluxes by the equation of continuity

$$\frac{\partial \phi_A(z)}{\partial t} = 0 = -\nabla J_A(z), \quad (14)$$

where  $J_A$  is the flux of segments  $A$ . Obviously, in the stationary state, the fluxes are independent of time and position. For simplification, we do not explicitly write the  $z$  dependence of the quantities in the following. We first present the derivation of the so-called slow-mode flux expression within the framework of the MFSD method. These fluxes will then be rewritten

in terms of Onsager coefficients. Using this short notation, the fast-mode flux expression can readily be derived.

#### 1. Slow-mode flux

The starting point is the Smoluchowski equation [35]:

$$\frac{\partial \phi_A}{\partial t} = \nabla \frac{1}{\zeta_A} (kT \nabla \phi_A + \phi_A \nabla U_A). \quad (15)$$

Here,  $\zeta_A$  is the monomer friction constant and  $U_A$  is the potential field felt by segments of type  $A$ . Two contributions to this potential can be distinguished:  $U_A(z) = E_A(z) + P(z)$ . There is a contribution  $E_A$  arising from molecular interactions with segments of other types:

$$E_A = kT \sum_B \chi_{AB} \langle \phi_B \rangle. \quad (16)$$

The other contribution  $P$  is a pressure term due to the requirement of incompressibility, which causes the fluxes of different segment types to be coupled.

Comparing the Smoluchowski equation with Eq. (14) yields for the flux of segments  $A$ :

$$J_A^s = -\frac{kT}{\zeta_A} \phi_A \left( \frac{1}{\phi_A} \nabla \phi_A + \nabla \sum_B \chi_{AB} \langle \phi_B \rangle + \frac{\nabla P}{kT} \right), \quad (17)$$

where we have substituted Eq. (16). The superscript  $s$  refers to the slow-mode approach.

The derivative of  $\phi_A$  is found by writing  $\phi_A(z, s)/C_A$  in Eq. (9) as  $G_A(z) \langle G_A(z, s-1|1) \rangle \langle G_A(z, s+1|N_A) \rangle$ :

$$\begin{aligned} \frac{\nabla \phi_A}{C_A} &= \nabla \left( G_A(z) \sum_s \langle G_A(z, s-1|1) \rangle \langle G_A(z, s+1|N_A) \rangle \right) \\ &\approx \sum_s \langle G_A(z, s-1|1) \rangle \langle G_A(z, s+1|N_A) \rangle \nabla G_A(z). \end{aligned} \quad (18)$$

In the last line, we used the so-called local coupling approximation (LCA), in which the kinetic coupling between segments is neglected: one segment of a chain is allowed to move independently from the motions of its neighbor segments. The LCA was also used by Fraaije in the density functional theory [9]. It might be a serious approximation (see Ref. [43] and references therein), but it allows efficient computation and analytical comparisons. Pair correlation functions or a completely different approach would be needed to avoid the LCA [43]. Substitution of Eq. (18) into the first term of Eq. (17) yields

$$\frac{\nabla \phi_A(z)}{\phi_A(z)} = \frac{1}{G_A(z)} \nabla G_A(z) = \nabla \ln G_A(z). \quad (19)$$

By inserting Eq. (19) and the well-known Einstein relation for the diffusion coefficient ( $D_A = kT/\zeta_A$ ) into Eq. (17) one arrives at

$$\begin{aligned}
J_A^s &= -D_A \phi_A \nabla \left( \ln G_A + \sum_B \chi_{AB} \langle \phi_B \rangle + \frac{P}{kT} \right) \\
&= -D_A \phi_A \nabla \left( \frac{\mu_A}{kT} + \frac{P}{kT} \right). \quad (20)
\end{aligned}$$

For the second version of Eq. (20), Eq. (8a) in the form  $u_A = -kT \ln G_A$  and Eq. (11) for  $\mu_A$  were used. The last unknown flux contribution  $\nabla P$  is obtained by requiring

$$\sum_A J_A(z) = 0 \quad \forall z \in [1, M], \quad (21)$$

which is the incompressibility constraint. From Eqs. (20) and (21) it is found that

$$\frac{\nabla P}{kT} = - \frac{1}{\sum_A D_A \phi_A} \sum_A D_A \phi_A \frac{\nabla \mu_A}{kT}. \quad (22)$$

Substituting this into Eq. (20) results after some rearrangement in the final expression for the slow-mode flux of segments  $A$ :

$$\begin{aligned}
J_A^s(z) &= - \frac{D_A \phi_A(z)}{\sum_C D_C \phi_C(z)} \sum_B D_B \phi_B(z) \nabla \left( \frac{\mu_A(z) - \mu_B(z)}{kT} \right). \\
&\quad (23)
\end{aligned}$$

## 2. Onsager coefficients

The flux is conveniently written in terms of Onsager coefficients  $\Lambda_A(z)$ , by which the single-chain dynamics enter the expressions for the collective dynamics. The Onsager coefficients as defined by Brochard [15] and Kramer [16] relate the unconstrained fluxes to their driving forces:

$$J_A^u = -\Lambda_A \nabla \mu_A. \quad (24)$$

The superscript  $u$  indicates that the incompressibility constraint is not yet taken into account. The Onsager coefficients are generally written in terms of segment mobilities  $B_A$ :

$$\Lambda_A = B_A \phi_A. \quad (25)$$

Combining this with Eq. (24) for the unconstrained flux and comparing the result with Eq. (20) where the constraint is given by the pressure term, it is found that  $B_A = D_A/kT = 1/\zeta_A$ . Using this relation for the mobility coefficient, the slow mode flux [Eq. (23)] may be written in terms of  $\Lambda$ 's as

$$\begin{aligned}
J_A^s &= - \frac{\Lambda_A}{\sum_C \Lambda_C} \sum_B \Lambda_B \nabla (\mu_A - \mu_B). \\
&\quad (26)
\end{aligned}$$

In Appendix A we show that this flux expression obeys Onsager's reciprocal relations.

The relation  $B_A = 1/\zeta_A$  is only valid for the Rouse regime. Other expressions for the mobility coefficients may also be used in Eq. (26). If a polymer chain is longer than the en-

tanglement length, Rouse behavior may no longer be assumed; the average mobility of the segments will decrease due to the entanglements. According to Ref. [15], this leads to a correction factor  $(N_e)_A/N_A$  so that  $B_A = (N_e)_A/(N_A \zeta_A)$ , where  $(N_e)_A$  is the *effective* entanglement length of  $A$  chains in the mixture. In pure  $A$ , the entanglement length equals  $N_{e0}$ . If the chains are diluted by monomeric solvents, the constraints to the segment motions are less pronounced than in pure  $A$ , so that the effective entanglement length may be approximated as  $(N_e)_A = N_{e0}[1 - \phi_{\text{monomer}}(z)]$ , where  $\phi_{\text{monomer}}$  is the total volume fraction of all monomer components.

Alternative expressions for the Onsager coefficient might be obtained by including the effect of chain connectivity (nonlocal coupling). Such Onsager coefficients are proportional to the pair-correlation function [8].

## 3. Fast-mode flux

The difference between the slow-mode model and the fast-mode model is the incorporation of vacancies. In the fast-mode model it is assumed that there exists a drift flux by the presence of vacancies

$$J_A^f = -\Lambda_A \nabla \mu_A + \phi_A J_{\text{vac}}. \quad (27)$$

To obey the condition of incompressibility [Eq. (21)], the flux of the vacancies is taken as  $J_{\text{vac}} = \sum_B \Lambda_B \nabla \mu_B$ , so that

$$J_A^f = - \sum_B (\phi_B \Lambda_A \nabla \mu_A - \phi_A \Lambda_B \nabla \mu_B). \quad (28)$$

The superscript  $f$  indicates that it concerns the flux in the fast-mode model. In Appendix A Onsager's reciprocal relations are verified.

## E. Four models

The combination of the multicomponent slow-mode flux [Eq. (26)] with the approximate segment chemical potentials [Eq. (13)] is a generalization of the binary model developed by Brochard, Jouffroy and Levinson [15]. We refer to this model as the B JL model. The combination of Eq. (26) with exact segment chemical potentials [Eq. (11)] is called the slow-mode SCF model or the SCF-B JL model. Combining Eq. (28) with the approximate segment chemical potentials is a generalization of the model developed by Kramer, Green and Palmström [16]. We refer to this model as the KGP model. The combination of Eq. (28) with exact segment chemical potentials is called the fast-mode SCF model or the SCF-KGP model.

## F. Procedure and Discretization

The stationary diffusion profiles are obtained by the following procedure. Segment weighting factors are calculated for mixtures *I* and *II* in accordance with the desired volume fractions in these bulk mixtures. Then the numerical iterations are started with an initial guess for the potentials  $u_A(z)$ . These are used to calculate the segment weighting factors within the diffusion layer. In this calculation the boundary

conditions (Sec. II G) play a role. The weighting factors enable the computation of the volume fractions [Eq. (9)]. These volume fractions are needed to check if the stop criteria for the stationary state are met. If not, a new iteration loop with newly chosen potentials  $u_A(z)$  is started. This is repeated until the the volume fractions obey the constraints. One constraint is a constant material flux for every component [Eq. (3d)]. Therefore, the flux equation needs to be written in discrete form for use in the lattice model. The continuity equation for a lattice with a one-dimensional gradient reads

$$\frac{\partial \phi_A(z)}{\partial t} = J_A(z-1 \rightarrow z) + J_A(z+1 \rightarrow z). \quad (29)$$

As an example, we take the slow-mode flux expression, Eq. (26), and rewrite it for convenience as

$$J_A^s(z) = \sum_B \Omega_{AB}(z) \nabla(\Delta \mu_{AB}(z)), \quad (30)$$

where  $\Delta \mu_{AB}$  is shorthand for  $\mu_A - \mu_B$ . Then  $J_A(z-1 \rightarrow z)$  in the lattice can be calculated as

$$J_A^s(z-1 \rightarrow z) = \frac{1}{2} \sum_B [\Omega_{AB}(z-1) + \Omega_{AB}(z)] \times \frac{\Delta \mu_{AB}(z) - \Delta \mu_{AB}(z-1)}{z - (z-1)}. \quad (31)$$

The stop criteria for the stationary diffusion become for all layers and for all components except one (say  $X$ ):

$$\begin{aligned} & \sum_B [\Omega_{AB}(z-1) + \Omega_{AB}(z)] [\Delta \mu_{AB}(z) - \Delta \mu_{AB}(z-1)] \\ & + [\Omega_{AB}(z) + \Omega_{AB}(z+1)] \\ & \times [\Delta \mu_{AB}(z+1) - \Delta \mu_{AB}(z)] = 0. \end{aligned} \quad (32a)$$

The stop criterion for component  $X$  is for all lattice layers:

$$\phi_X(z) = 1 - \sum_B \phi_B(z). \quad (32b)$$

### G. Boundary conditions

The boundaries of the diffusion layer deserve some extra attention. Behind the boundaries ( $z \leq 0$  and  $z \geq M+1$ ) are bulk mixtures with specified volume fractions  $\phi_A^I$  and  $\phi_A^{II}$ . A property of any bulk system is the condition that  $G_A^b(z) = \text{constant} = \langle G_A^b(z) \rangle$ . As a result,  $G_A^b(z, s|1) = (G_A^b)^s$  and  $G_A^b(z, s|N_A) = (G_A^b)^{N_A - s + 1}$ . For homopolymers or monomers  $G_A^b$  is known:

$$G_A^b = \left( \frac{\phi_A^b}{\phi_A^{\text{ref}}} \right)^{1/N_A}. \quad (33)$$

We choose to have an abrupt transition between the bulk mixtures and the system; if  $z=1$  is the first layer in the system, then  $z=0$  represents a true bulk. The consequence is

an inconsistency at the boundaries and some ‘‘forbidden’’ chain conformations, which will be discussed in a future publication. All results presented in this paper are obtained from the ‘‘abrupt transition conditions.’’ We have used other boundary conditions as well [e.g., mirrors for the calculation of  $\phi$  combined with bulk conditions for the calculation of the driving forces, or taking  $G_A(z \leq 0, s) = G_A^I$  and  $G_A(z \leq 0, s|1)$  still depend on  $G_A(z > 0, s^* < s, 1)$ ], but the influence on the resulting diffusion profiles are negligible.

### H. Diffusion coefficients

An advantage of using the approximate segment chemical potentials is that the flux-expressions in terms of  $\mu$  gradients can easily be rewritten in terms of  $\phi$  gradients. This allows the analytical description of the stationary diffusion profiles for some simple systems. Since we only consider athermal systems in the following and since we wish to avoid unnecessary multiline equations, we assume that  $\chi_{AB} = 0$  for all  $A, B$  in the present paragraph. Generally, the flux expression in terms of  $\phi$  gradients reads

$$J_A = - \sum_B \tilde{D}_{AB}^{(X)} \nabla \phi_B \quad (34)$$

by which the mutual diffusion coefficients are defined. The superscript  $X$  indicates that all volume fractions, except that for the component containing segment type  $X$ , are taken as the independent variables for the flux. For example, the flux of segments  $A$  in a binary ( $A/B$ ) system can be written in two ways:

$$J_A = - \tilde{D}_{AA}^{(B)} \nabla \phi_A = - \tilde{D}_{AB}^{(A)} \nabla \phi_B. \quad (35)$$

Brochard [15] derived for the mutual diffusion coefficient  $\tilde{D}_{AA}^{(B)}$  for athermal binary systems:

$$\frac{\tilde{D}_{AA}^{(B)}}{kT} = \frac{\Lambda_A \Lambda_B}{\Lambda_A + \Lambda_B} \left( \frac{1}{\phi_A N_A} + \frac{1}{\phi_B N_B} \right). \quad (36)$$

As discussed in Sec. I,  $(\tilde{D}_{AA}^{(B)})^{-1}$  is proportional to  $(1/\Lambda_A + 1/\Lambda_B)^{-1}$ . By substituting Eq. (13) into the slow-mode flux equation (26) and after some rearrangement, the mutual diffusion coefficients for multicomponent systems in the BJL model are found to be

$$\frac{\tilde{D}_{AB}^{s(X)}}{kT} = \frac{\Lambda_A}{\sum_C \Lambda_C} \left[ \frac{\Lambda_X}{\phi_X N_X} - \frac{\Lambda_B}{\phi_B N_B} - \sum_Q \frac{\Lambda_Q}{\phi_A N_A} (\delta_{AX} - \delta_{AB}) \right]. \quad (37)$$

It is easily shown that for binary systems Brochard’s mutual diffusion coefficient is recovered.

The mutual diffusion coefficients for the Kramer model are obtained by inserting Eq. (13) into the fast-mode flux equation (28):

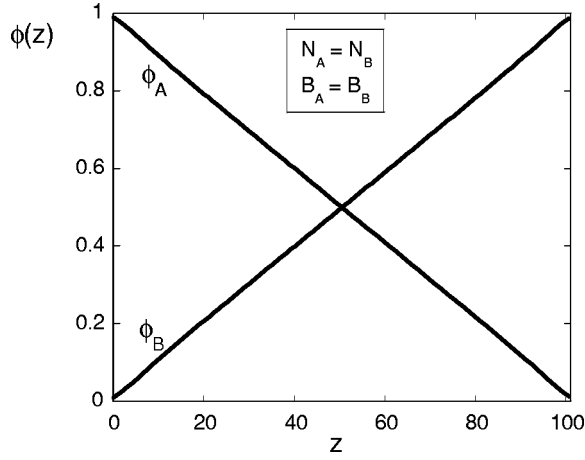


FIG. 2. Stationary diffusion profiles in a binary system calculated with four different models.  $N_A = N_B = N_{e0} = 100$ ,  $B_A = B_B = 1$ . All four models give the same result, with linear profiles.

$$\begin{aligned} \frac{\tilde{D}_{AB}^{f(X)}}{kT} = & \left( \phi_A \sum_C \Lambda_C - \Lambda_A \right) \left( \frac{1}{N_B} - \frac{1}{N_X} \right) \\ & - \phi_A \left( \frac{\Lambda_B}{\phi_B N_B} - \frac{\Lambda_X}{\phi_X N_X} \right) - \frac{\Lambda_A}{\phi_A N_A} (\delta_{AX} - \delta_{AB}) \end{aligned} \quad (38)$$

so that  $\tilde{D}_{AB}^{f(X)}$  is a linear combination of  $\Lambda$ 's.

Obviously, if  $\phi_X$  is not an independent variable of the flux,  $\tilde{D}_{XX}^{(X)}$  and  $\tilde{D}_{AX}^{(X)}$  should vanish, which is satisfied by Eqs. (37) and (38).  $\tilde{D}_{AA}^{(X)}$  is always positive for  $X \neq A$ . For binary systems  $\nabla \phi_A = -\nabla \phi_B$ , thus according to Eq. (35), we must find that  $\tilde{D}_{AA}^{(B)} = -\tilde{D}_{AB}^{(A)}$ , which can also be verified by Eqs. (37) and (38).

### III. RESULTS

We illustrate the concepts of the MFSD method by showing the stationary diffusion profiles for various athermal systems. Stationary diffusion profiles are the volume fractions for each component as a function of the spatial parameter  $z$ , such that the two bulk mixtures have the desired composition and such that there is no accumulation of material anywhere between these bulk mixtures. We stress again that the stationary solution is the only solution of the MFSD method. We do not obtain the stationary profiles by following the physical trajectories towards the steady state, but directly by computing the volume fraction profiles that obey all conditions for the steady state. As outlined before, the method has been applied for four different diffusion models. We treat binary and multicomponent systems separately. All binary systems considered in this study have the boundary conditions  $\phi_A^I = 0.99$  and  $\phi_A^II = 0.01$ . First, the results are presented. After that, an attempt to rationalize them is given.

The most simple systems to study stationary diffusion are those for which all components have the same chain length  $N$  and the same mobility  $B$ . Figure 2 presents the MFSD stationary diffusion profile for such a system. It is seen that

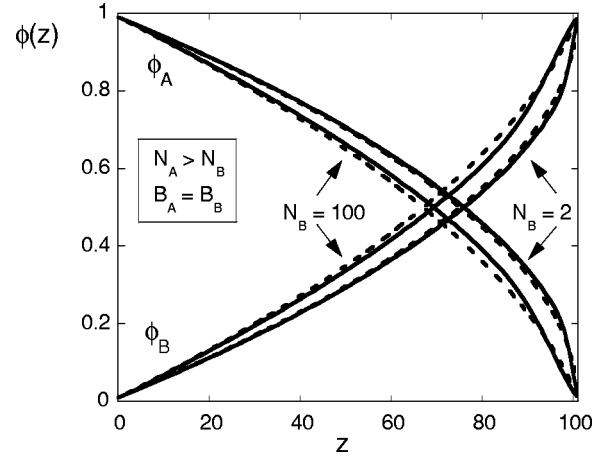


FIG. 3. Stationary diffusion profiles in two binary systems calculated with four different models.  $N_A = 500$ ,  $N_B = 100$  or  $2$ ,  $1/\zeta_A = 5$ ,  $1/\zeta_B = 1$ ,  $N_{e0} = 100$  so that  $B_A = B_B = 1$ . Solid lines correspond to calculations with SCF-potentials (SCF-BJL and SCF-KGP), dashed lines correspond to approximate potentials (BJL and KGP).

these simple systems give rise to linear volume fraction profiles in the stationary state, independent of the model used. The linear profiles turn into convex profiles if the components have either different  $N$  or different  $B$ , as shown in Figs. 3 and 4, respectively.

In Fig. 3 we have plotted the stationary diffusion profiles for two systems: one system has  $N_A/N_B = 5$ , and the other has  $N_A/N_B = 250$ . This figure shows that the BJL and KGP results (dashed curves) coincide if the components only differ in their chain lengths. The SCF-BJL and SCF-KGP models (solid curves) also yield indistinguishable profiles for such systems. However, the exact calculation of segment chemical potentials yields profiles which slightly differ from those calculated by approximated segment chemical potentials, in particular, for increasing  $\phi$  gradients and decreasing  $N_A/N_B$ . The discrepancy at large  $\nabla \phi$  is a result of the assumption of homogeneous mixtures in the Flory-Huggins expression for the approximated chemical potential. It is seen that the larger the ratio between the chain lengths, the more convex the profiles. The volume fractions change rapidly near the bulk mixture that contains a large amount of short (and therefore, for given segment mobilities, more mobile) chains.

If the chain lengths are the same, while the segment mobilities are different, the profiles no longer coincide for any of the four models, as shown in Fig. 4. For these systems, it is the diffusion mechanism (slow- or fast-mode) that mainly determines the stationary diffusion profiles; it is less important whether the segment chemical potentials are calculated exactly or not: KGP profiles compare very well with SCF-KGP profiles [Fig. 4(a)], and BJL profiles are similar to SCF-BJL profiles [Fig. 4(b)]. Since we have combined the profiles for two different systems in Figs. 4(a) and 4(b) (namely, for  $B_B/B_A = 5$  and  $B_B/B_A = 250$ ), it can directly be seen that the slow-mode expression is more sensitive to the segment mobilities than the fast-mode expression. The volume fractions change rapidly near the bulk mixture that contains a large amount of components consisting of relatively mobile seg-

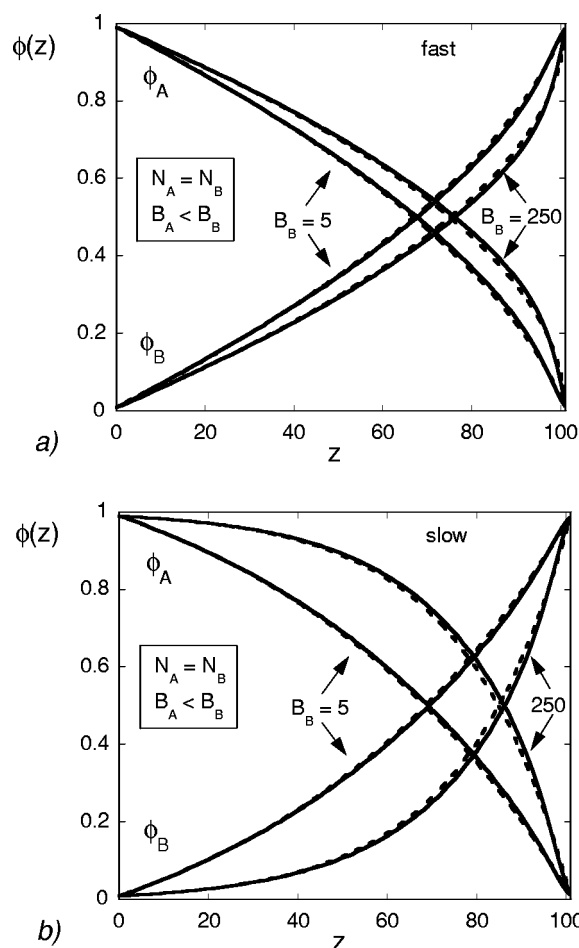


FIG. 4. Stationary diffusion profiles in two binary systems calculated with four different models.  $N_A = N_B = N_{e0} = 100$ ,  $B_A = 1$ , and  $B_B = 5$  or  $250$ . Solid curves correspond to SCF potentials, dashed ones correspond to approximate potentials. Part (a) is obtained by the two fast-mode models, part (b) by the slow-mode models.

ments. This behavior is more pronounced when the ratio between segment mobilities increases.

Comparing Figs. 3 with 4(a), it appears that longer chains act like less mobile components. In particular, the stationary diffusion profiles calculated by the KGP model were found to be exactly the same for two binary systems ( $\alpha$ ) and ( $\beta$ ) if  $(N_A/N_B)^{(\alpha)} = (B_B/B_A)^{(\beta)}$  while  $(B_B/B_A)^{(\alpha)} = 1 = (N_A/N_B)^{(\beta)}$ . In other words, a system containing two components with different chain lengths but equal segment mobilities may be simulated by a system containing two monomers (or two polymers of the same length) with different segment mobilities. This is only true for the KGP model. This may suggest that the lower mobility of longer chains might be compensated by a higher mobility of its constituting segments. It would then be expected that the components would act as mutually indistinguishable if the system parameters were chosen such that  $N_A/N_B = B_A/B_B$ . Indistinguishable components would result in linear profiles (cf. Fig. 2). Figure 5 shows that this is true for the two slow-mode models, but not for the fast-mode models. Note that the fast-mode results differ significantly when the exact segment chemical poten-

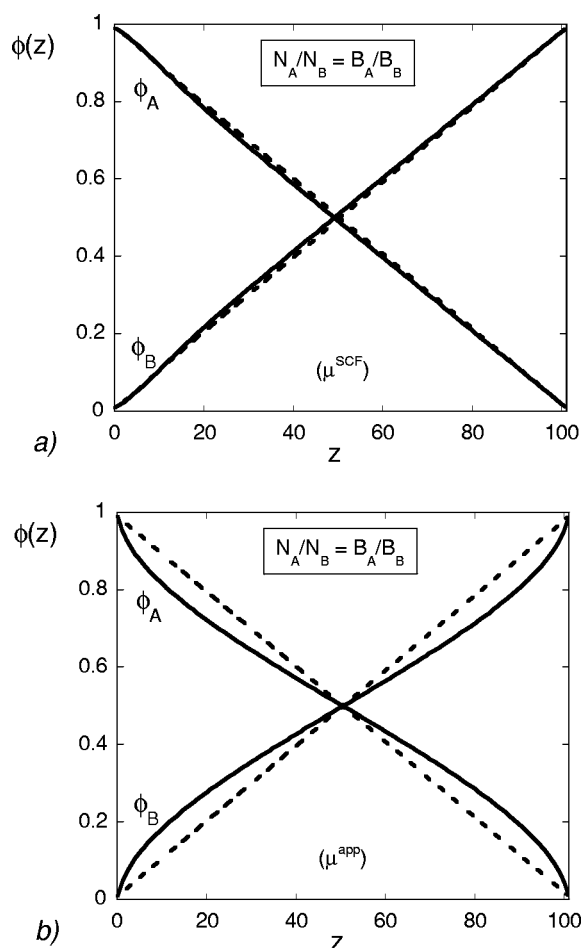


FIG. 5. Stationary diffusion profiles in a binary system calculated with four different models.  $N_A = 10$ ,  $N_B = N_{e0} = 500$ ,  $B_A = 1$ ,  $B_B = 50$ , so that  $N_A/N_B = B_A/B_B$ . Solid curves are calculated by the fast-mode models and dashed ones are calculated by the slow-mode models. For part (a) SCF-potentials are used, for part (b) approximate potentials.

tials are replaced by approximate ones. The discrepancy does not only occur for the largest  $\phi$  gradients. The comparison between the models for other choices of parameters generally yields the same conclusions as derived from Fig. 5: usually the slow-mode results are less affected by the way to calculate the segment chemical potentials than the fast-mode results.

The four variants of the MFSD method were also used to calculate the stationary diffusion profiles for ternary systems: two equally long polymers in a solvent. The differences between the models are too small to be observed in the systems presented in Fig. 6. This figure shows three systems that differ only slightly in the imposed volume fractions at the left-hand boundary ( $z=0$ ):  $\phi_B(0)=0.1$  in all cases and  $\phi_A(0)=0.75$  (top),  $0.8$  (middle), and  $0.85$  (bottom). It is seen that these small differences result in very different profiles. The solvent (monomer) has a rather flat and approximately linear profile in all cases. The largest  $\phi$  gradients of the polymers are found at the highest monomer concentration.

Another striking example of a ternary system is presented

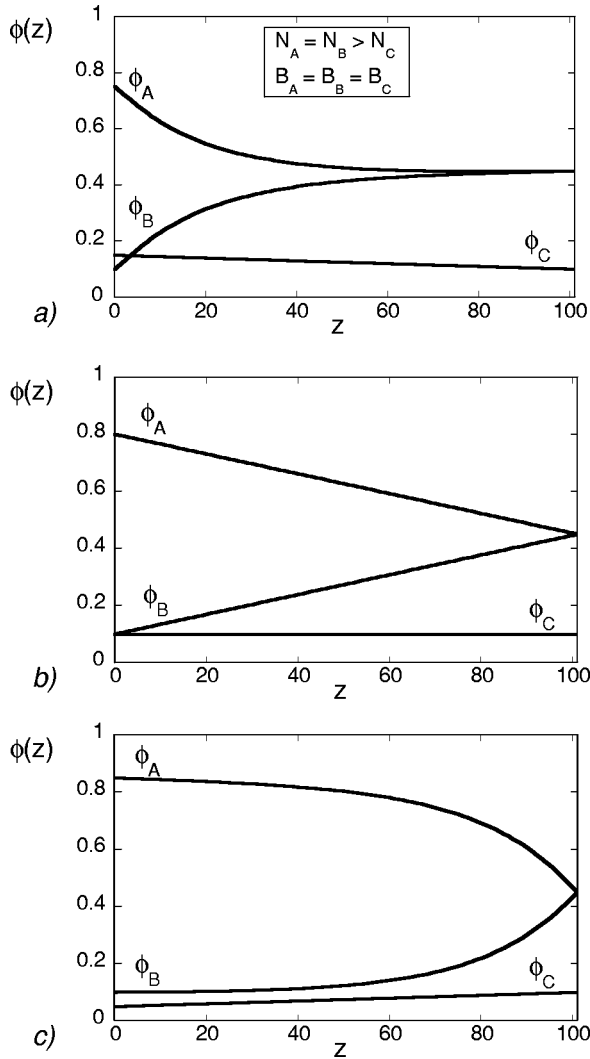


FIG. 6. Stationary diffusion profiles in a ternary system containing two homopolymers ( $A$  and  $B$ ) and one monomer ( $C$ ).  $N_A = N_B = N_{e0} = 100$ ,  $N_C = 1$ ,  $B_A = B_B = B_C = 1$ . The only parameters that were varied in systems (a)–(c) are  $\phi_A(0)$  and  $\phi_C(0)$ . All models give essentially the same results.

in Fig. 7. Despite the fact that the imposed values for  $\phi_A$  are the same at both sides of the system [ $\phi_A(0) = \phi_A(M+1)$ ], this component has large gradients within the system. The profiles are the same for the fast- and slow-mode calculations, as was the case for binary systems in which all segments had the same mobilities. Small differences occur if the segment chemical potentials are not calculated exactly. However, the longer the polymer chains, the larger the differences (not shown).

As explained in Sec. II G, our boundary conditions are such that in the vicinity of the bulk mixtures some chain conformations could not occur. The stationary diffusion profiles do not suffer from these boundary conditions; the profiles scale accordingly with the system size as long as the system is not too small in comparison with the chain lengths. This is shown in Fig. 8, where we plotted the diffusion profiles versus the normalized distance parameter  $z/(M+1)$ . The diffusion profiles are not influenced by the size of the

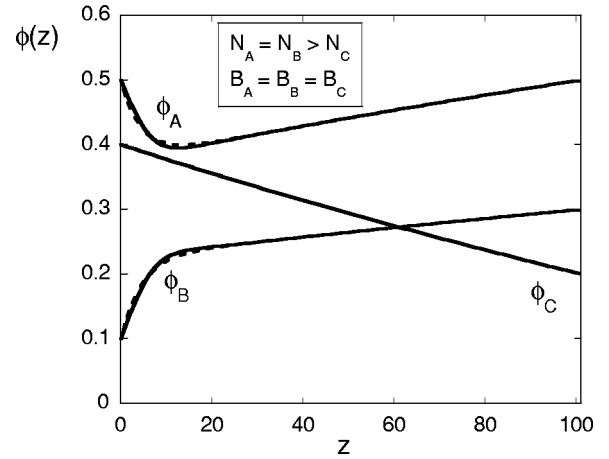


FIG. 7. Stationary diffusion profiles in a ternary system containing one monomer ( $C$ ) and two homopolymers ( $A$  and  $B$ ) with equal chain lengths and segment mobilities, and equal  $\phi_A$  but different  $\phi_B$  at the boundaries. Note that  $\phi_A(0) = \phi_A(M+1)$ .  $N_A = N_B = N_{e0} = 100$ ,  $N_C = 1$ ,  $B_A = B_B = B_C = 1$ . Solid curves are obtained by the SCF potentials and dashed ones are obtained by approximate potentials. No difference is found between the fast- or slow-mode mechanism.

system if  $M \approx N$ , where  $N$  is the length of the longest polymer chains. Note that we find oscillating volume fraction profiles if the chains are long compared to the system size ( $N=400$ ,  $M=100$ ) and when the driving forces are calculated exactly. Using the approximate segment chemical potentials does not give oscillating profiles.

#### IV. DISCUSSION

From Eqs. (26) and (28) it is easily concluded that the slow-mode and fast-mode models are indistinguishable for  $\Lambda_A(z)/\phi_A(z) = \Lambda_B(z)/\phi_B(z) \forall A, B, z$ , which means  $B_A(z) = B_B(z) = B(z) \forall A, B, z$ . This can only be true if  $B$  is inde-

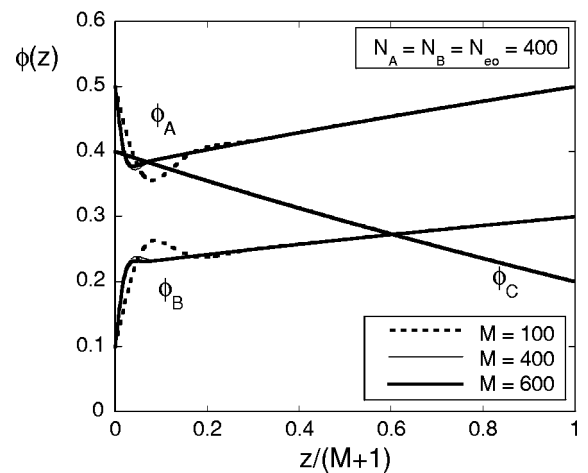


FIG. 8. The same system as in Fig. 7 for longer chains ( $N_A = N_B = N_{e0} = 400$ ) and for various system sizes  $M$ , calculated by the SCF potentials. Volume fractions are now plotted vs the normalized  $z$  variable. Increasing the system size above  $M=N$  does not change the shape of the profiles significantly.

TABLE I. Stationary binary systems:  $\phi$  derivatives of the diffusion coefficients and  $\phi$  gradients. The expressions for  $\tilde{D}_{AA}^{(B)}$  were obtained from Eqs. (36)–(38) after inserting  $\Lambda_A = B_A \phi_A$  and  $\Lambda_B = B_B \phi_B$  [Eq. (25)].

|                |   | $N_A = N_B = N$<br>$B_A = B_B = B$<br>(Fig. 2) | $N_A = xN_B$<br>$B_A = B_B = B$<br>(Fig. 3)    | $N_A = N_B = N$<br>$B_B = xB_A$<br>(Fig. 4)           |
|----------------|---|--|--|---|
| BJL model [15] | $\tilde{D}_{AA}^{(B)}$                                  | $\frac{BkT}{N}$                                | $\frac{BkT}{N_A}(\phi_B + x\phi_A)$            | $\frac{B_B kT}{N} \frac{1}{(\phi_A + x\phi_B)}$       |
|                | $\frac{\partial \tilde{D}_{AA}^{(B)}}{\partial \phi_A}$ | 0  | $\frac{BkT}{N_A}(x-1)$                         | $\frac{B_B kT}{N} \frac{(x-1)}{(\phi_A + x\phi_B)^2}$ |
|                | $\frac{\partial  \nabla \phi_A }{\partial \phi_A}$      | 0  | $< 0$ for $N_A > N_B$<br>$> 0$ for $N_A < N_B$ | $< 0$ for $B_A < B_B$<br>$> 0$ for $B_A > B_B$        |
| KGP model [16] | $\tilde{D}_{AA}^{(B)}$                                  | $\frac{BkT}{N}$                                | $\frac{BkT}{N_A}(\phi_B + x\phi_A)$            | $\frac{B_A kT}{N}(\phi_B + x\phi_A)$                  |
|                | $\frac{\partial \tilde{D}_{AA}^{(B)}}{\partial \phi_A}$ | 0  | $\frac{BkT}{N_A}(x-1)$                         | $\frac{B_A kT}{N}(x-1)$                               |
|                | $\frac{\partial  \nabla \phi_A }{\partial \phi_A}$      | 0  | $< 0$ for $N_A > N_B$<br>$> 0$ for $N_A < N_B$ | $< 0$ for $B_A < B_B$<br>$> 0$ for $B_A > B_B$        |

pendent of  $z$ . Figures 2, 3, 7, and 8 show that this exact agreement between the slow- and fast-mode models is indeed found. In the remainder of this discussion, we first discuss some analytical descriptions and then focus on the general characteristics of binary and multicomponent systems.

### A. Comparison with analytical results

Due to our choice of simple systems, we can compare the MFSD results with analytical results. Analytical expressions for  $\phi_A(z)$  are obtained by solving Eq (34) in combination with the diffusion coefficients of either the BJL model or the KGP model.

Suppose that all components have the same mobility  $B$  (so that the BJL and KGP models are identical) and the same chain length  $N$ . The flux is then simply given by  $J_A(z) = -(BkT/N)\nabla \phi_A(z) \forall A, z$ . To satisfy the condition of constant fluxes, the analytical expressions for  $\phi$  are linear functions of  $z$ . The MFSD result obeys this linear behavior for all four models, as shown in Fig. 2.

For binary systems  $\phi_A(z)$  can be obtained by solving  $-\int \tilde{D}_{AA}^{(B)} d\phi_A = J_A z + k_1$ . Expressions for  $\tilde{D}_{AA}^{(B)}$  for various simple cases are given in Table I. When  $B_A = B_B$  and  $N_A \neq N_B$ ,  $\tilde{D}_{AA}^{(B)}$  is given by  $\tilde{D}_{AA}^{(B)} = a - b\phi_A$  with  $a = BkT/N_A$  and  $b = BkT(1/N_A - 1/N_B)$ . The result for  $N_A > N_B$  is

$$\phi_A(z) = \frac{a}{b} - \frac{1}{b} \sqrt{a^2 + 2b(k_1 + J_A z)}. \quad (39)$$

The integration constant  $k_1$  and the flux  $J_A$  can be found from the known values of  $\phi_A(0)$  and  $\phi_A(M+1)$ . Due to the

condition that  $N_A > N_B$ , the sign of the square root term is unambiguously determined. The volume fraction profile of the short-chain component simply follows from  $\phi_B = 1 - \phi_A$ .

In case of equal chain lengths but  $B_A \neq B_B$ , we find for the BJL model  $\tilde{D}_{AA}^{(B)} = a/(c\phi_A + B_B)$ , with  $a = B_A B_B kT/N$  and  $c = B_A - B_B$ . Thus, for  $B_B > B_A$ , the stationary volume fraction profile is

$$\phi_A(z) = \frac{k_2}{c} \exp\left\{-\frac{cJ_A}{a}z\right\} - \frac{B_B}{c} \quad (40)$$

with  $k_2 = \exp\{-ck_2/a\}$ . The same system has for the KGP model  $\tilde{D}_{AA}^{(B)} = a - c\phi_A$  with  $a = B_A kT/N$  and  $c = (B_A - B_B)kT/N$ , so that

$$\phi_A(z) = \frac{a}{c} - \frac{1}{c} \sqrt{a^2 + 2c(k_3 + J_A z)}. \quad (41)$$

It is not possible to find analytically an explicit expression for  $\phi_A(z)$  if both the chain lengths and the segment mobilities are chosen arbitrarily. In Fig. 9 analytical expressions (39)–(41) are plotted together with the corresponding results from the MFSD method. They match each other exactly.

In Appendix B, we show that for the three-component system in Fig. 7 with  $B_A = B_B = B_C$ ,  $N_A = N_B$ , and  $N_A > N_C$ , the analytical expressions for the volume fractions read

$$\phi_A(z) = \frac{aJ_A}{bJ_C} [d(z) - 1] + k_5 \exp\{-d(z)\},$$

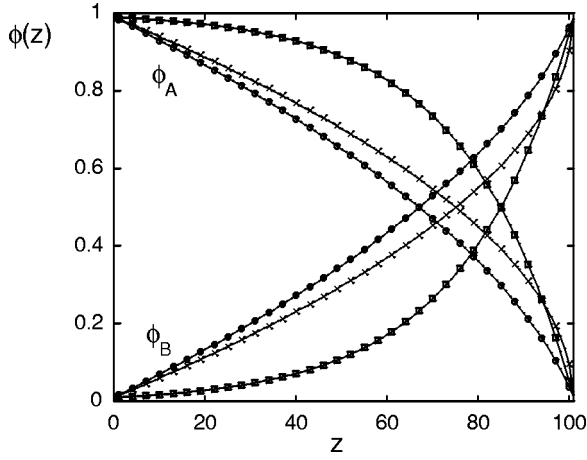


FIG. 9. Comparison of results from the MFSD method (markers) with the corresponding analytical results (curves) in different binary systems. In all cases  $M=100$ ,  $N_B=100$ , and  $B_A=1$ . The circles are for the BJL and KGP model with  $N_A/N_B=5$  and  $B_A=B_B$ . The squares are for the BJL model with  $N_A=N_B$  and  $B_B/B_A=250$ . The crosses are for the KGP model with  $N_A=N_B$  and  $B_B/B_A=250$ .

$$\phi_B(z) = \frac{aJ_B}{bJ_C} [d(z) - 1] - k_5 \exp\{-d(z)\}, \quad (42)$$

$$\phi_C(z) = \frac{a}{b} [d(z) - 1] + 1,$$

where  $a = BkT/N_A$ ,  $b = BkT(1/N_A - 1/N_C)$ ,  $d(z) = 1/a\sqrt{s+tz}$ ,  $s = a^2 + 2bk_4$ ,  $t = -2bJ_C$  and  $J_C = -J_A - J_B$ .  $J_A$ ,  $J_B$  and the integration constants  $k_4$  and  $k_5$  are given by the compositions of the bulk mixtures. These equations reproduce the profiles in Fig. 7 (including the minimum in  $\phi_A$ ) with the same accuracy as shown for binary systems in Fig. 9.

The exact agreement between the analytical profiles and the MFSD results proves the proper performance of the MFSD method. In addition, they show that the abrupt transition between the system and the bulk mixtures in the MFSD method does not disturb the diffusion profiles. However, if the system is small compared to the longest chains, small discrepancies may occur between the analytical results and the MFSD results.

### B. General characteristics of binary systems

We now focus on general characteristics of the diffusion profiles for binary systems. It is convenient to analyze how  $\nabla\phi$  should change with  $\phi$  according to the flux expressions for the approximate models, since this behavior of  $\nabla\phi$  can readily be checked by plots of diffusion profiles. Since  $\nabla\phi_A = -J_A/\tilde{D}_{AA}^{(B)}$  and  $J_A = \text{constant}$ , we have

$$\frac{\partial\nabla\phi_A}{\partial\phi_A} = -\frac{\nabla\phi_A}{\tilde{D}_{AA}^{(B)}} \frac{\partial\tilde{D}_{AA}^{(B)}}{\partial\phi_A}. \quad (43)$$

Given that  $\tilde{D}_{AA}^{(B)}$  is positive, it is concluded that for binary systems  $\partial\tilde{D}_{AA}^{(B)}/\partial\phi_A$  and  $\partial|\nabla\phi_A|/\partial\phi_A$  must have opposite signs. In Table I different classes of binary systems are distinguished by different combinations of parameters. For each class and for both approximate models the sign of  $\partial|\nabla\phi_A|/\partial\phi_A$  is evaluated by first writing the general expression for  $\tilde{D}_{AA}^{(B)}$  and then calculating its derivative with respect to  $\phi_A$ . We first note that the KGP model yields the same stationary diffusion profiles for the second (Fig. 3) and third (Fig. 4) classes if  $(N_A/N_B)_{\text{equal } B} = (B_B/B_A)_{\text{equal } N}$ , as can be seen from the diffusion coefficients in the second and third columns of Table I. This implies that the mobility of a chain can effectively be changed by either its chain length or the segment mobility. The general conclusion that can be drawn from Table I is that the larger the fraction of relative mobile component, the steeper the volume fraction profiles for stationary diffusion: it is observed that  $\partial|\nabla\phi_A|/\partial\phi_A$  is positive if  $\phi_A$  is the relative mobile component. The first column shows that if both components have the same mobilities, the gradients of the volume fractions are constant. The second column implies an increasing  $\nabla|\phi|$  for increasing volume fraction of the shorter, and therefore more mobile, homopolymer. These columns refer to classes of systems for which the slow-mode and the fast-mode fluxes are the same, in accordance with previous statements. The third column in Table I refers to systems for which the slow-mode and fast-mode models no longer coincide, but the general conclusion remains valid for both models.

Barrer [44] and Crank [45] also present stationary diffusion profiles for concentration-dependent diffusion coefficients. Their general conclusion is that the concentration profiles are convex towards the  $z$  axis if  $\partial\tilde{D}_{AA}^{(B)}/\partial c_A < 0$ , and convex away from the  $z$  axis if  $\partial\tilde{D}_{AA}^{(B)}/\partial c_A > 0$ . Our results are in agreement with their conclusion, but we can state more specifically that the profiles are convex towards the  $\phi$  axis if  $\partial\phi^{\text{fast}}/\partial z < 0$  and vice versa, where  $\phi^{\text{fast}}$  refers to the relative mobile component. This general behavior can be understood by considering how these stationary profiles develop from the initial profile at  $t=0$ , which is assumed to be discontinuous at  $z = \frac{1}{2}M$  [see Fig. 10(a)]. Suppose the major component at the left side of the system consists of relative mobile  $A$  segments, whereas at the right side mainly low-mobile  $B$  segments are present. From Table I it follows that  $\partial\tilde{D}/\partial\phi^{\text{fast}} < 0$  so that the diffusion coefficient is smaller at the left than at the right. Segments  $A$  start diffusing to the right by exchanging their positions with segments  $B$ . At first instance, the  $\phi$  gradients at both sides will be similar:  $\nabla\phi_A(z = \frac{1}{2}M - \epsilon) \approx \nabla\phi_A(z = \frac{1}{2}M + \epsilon)$  [Fig. 10(b)]. However, the gradient at  $z = \frac{1}{2}M + \epsilon$  vanishes more rapidly than at  $z = \frac{1}{2}M - \epsilon$  due to the larger diffusion coefficient [Fig. 10(c)]. This results in flatter profiles at low concentration of mobile component.

Comparing the approximate models with the exact models, we found two situations in which discrepancies may occur. First, discrepancies occurred if the system was small compared to the chain lengths. The oscillations in Fig. 8 were only found if the driving forces are calculated by the

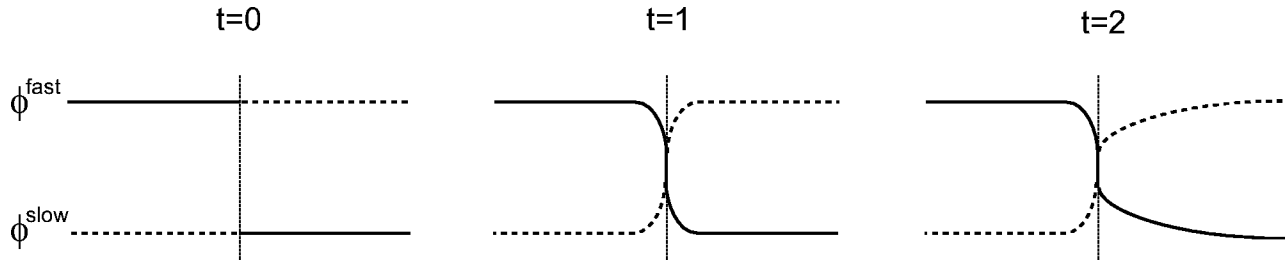


FIG. 10. Schematic picture of the developing diffusion profiles for fast component diffusing to the right and slow component to the left.

exact segment chemical potentials and if the chains are long compared to the system size. The smaller the system or the longer the chains, the larger the gradients in the region in which the chains find themselves. In other words, the assumption of local homogeneity, as used for the approximate segment chemical potentials, is incorrect for such small systems with long chains. Second, discrepancies between approximate and exact *fast-mode* calculations occurred if the components had both dissimilar chain lengths and dissimilar segment mobilities (e.g., Fig. 5). In general, agreement was found between BJL and SCF-BJL for such systems. In other words, the fast-mode model seems to be more sensitive to the calculation of the driving force than the slow-mode model. Probably, the error in  $\nabla\mu_A$  is compensated by the error in  $\nabla\mu_B$  in calculations applying the slow-mode fluxes, since the driving forces appear as  $\nabla(\mu_A - \mu_B)$  in these flux expressions [cf. Eq. (26)]. On the contrary, in the KGP model, the errors in  $\nabla\mu$  are weighted by segment mobilities due to the terms  $B_A\nabla\mu_A - B_B\nabla\mu_B$  in the flux expressions [Eq. (28)].

### C. General characteristics of multicomponent systems

Figure 6 can now be understood from Table I. Since the homopolymer components in Fig. 6(b) are indistinguishable, the chemical potential of the monomer component is constant. Effectively, this system refers to binary diffusion of two homopolymers with equal chain lengths and mobilities, for which the profiles must be linear. At first instance, Figs. 6(a) and 6(c) may also be interpreted as the stationary diffusion profiles for binary mixtures, one component being the monomer, the other the combination of both polymers. Indeed, as predicted by Table I, the profiles change rapidly at high monomer concentrations. This is true not only for the monomer and the total of the two polymers, but also for the individual polymer components. This can be understood from the observation that the polymers are identical and they have a similar absolute difference between  $\phi^I$  and  $\phi^{II}$ . As a result, they must behave similarly and with opposite gradients.

A first remark for the three-component system in Fig. 7 concerns the behavior of polymer A. Despite the equal volume fractions in both bulk mixtures, its volume fraction within the system is not constant. Due to the requirement of stationary diffusion, the flux of segments A needs to be constant throughout the system. For this particular system,  $J_A$  is found to be negative; A segments diffuse from the right to the left. This implies that for small values of  $z$  the A seg-

ments diffuse against a concentration gradient. This phenomenon is called “uphill diffusion.” It is found only in multicomponent systems and must be due to either diffusive coupling of components (large  $|\tilde{D}_{AB}^{(X)}|$  for  $A \neq B$ ) or negative “main diffusion coefficients” ( $\tilde{D}_{AA}^{(X)} < 0$ ). In our system,  $\tilde{D}_{AA}^{s(C)} = \tilde{D}_{AA}^{f(C)} = \phi_A[1/N_C + \phi_B/(\phi_A N_A)] \approx \phi_A > 0$  and  $\tilde{D}_{AB}^{s(C)} = \tilde{D}_{AB}^{f(C)} = \phi_A[1/N_C - 1/N_B] \approx \phi_A$  [see Eqs. (37) and (38)]. The relatively large cross diffusion coefficient  $\tilde{D}_{AB}^{(C)}$  drives the flux of A segments towards the region of low  $\phi_B$ . Experimental evidence for uphill diffusion has been reported frequently for metallic systems and in the context of geological studies [46–48] in which all diffusing components have nearly equal sizes. Negative main diffusion coefficients have been measured in ternary surfactant mixtures [49]. Uphill diffusion has been found in theoretical studies as well [50,13], for example, as a result of interparticle interactions. We are not aware of any reports on uphill diffusion only due to chain-length effects. (Remind that we consider athermal systems.) Note that A segments have  $\phi_A(0) = \phi_A(M+1)$ , but  $\mu_A^{chain}(0) < \mu_A^{chain}(M+1)$ , as a result of the different monomer contents at both sides.

The profile of the monomer can be understood by considering the system as a binary mixture, since the polymers are indistinguishable. The monomer concentration must therefore change rapidly at the left side, where its concentration is maximal.

## V. CONCLUSIONS

The equilibrium Scheutjens-Fleer method has been extended to create a new framework for the modeling of stationary diffusion in polymer systems. The numerical algorithm converges fast and smoothly to stationary volume fraction profiles that obey the imposed volume fractions at the system boundaries. It is important to note that, although we implemented the transition between the bulk mixtures and the gradients in a rather rough way, the diffusion profiles did not suffer from it. Two theories, presented in the literature for binary homopolymer diffusion and referred to as “slow mode” and “fast mode,” respectively, were combined with two methods to calculate the segment chemical potentials. This yielded four models for the fluxes. The parameters for the flux equations are the Flory-Huggins interaction parameters  $\chi$ , the chain lengths of the components  $N_A$ , the entanglement length of the components  $N_e$ , and the mobilities of the constituent segments  $1/\zeta_A$ . In general, the diffu-

sion profiles were more sensitive to the applied theory (slow mode or fast mode) than to the calculation of segment chemical potentials. However, results from the two slow-mode models are more similar than those from the two fast-mode models. By analytical analysis of diffusion coefficients, we were able to verify the usually asymmetric diffusion profiles. We have thereby verified the MFSD method since the analytical results matched exactly the results from the MFSD method. It has been found for stationary diffusion profiles that the volume fractions change more rapidly at the location where the amount of mobile components is larger. The mobility of components is determined both by the segment mobilities and by their chain lengths. We only studied athermal systems, but mutually interacting components might be studied as well by the MFSD method. It is, therefore, possible to study interfaces in the presence of concentration gradients, as well as diffusion through pores of membranes that energetically interact with some components. Another interesting aspect of the MFSD method is that it provides information about the chain conformations; this information was not discussed in the present paper and will be presented elsewhere.

#### ACKNOWLEDGMENTS

This research was financially supported by the Council for Chemical Sciences of the Netherlands Organization for Scientific Research (CW-NWO) via the program Computational Materials Science.

#### APPENDIX A: ONSAGER'S RECIPROCAL RELATIONS

Mass transport driven by chemical potential gradients may be written in the standard form of Onsager's phenomenological equations

$$J_A = - \sum_B L_{AB} \nabla \mu_B, \quad (\text{A1})$$

where  $L_{AA}$  are the main transport coefficients and  $L_{AB}$  are the cross coefficients describing the coupling between the fluxes. According to Onsager's reciprocal relations we should have  $L_{AB} = L_{BA} \forall A, B$ .

The slow-mode flux of Eq. (26) may be written in the form of Eq. (A1) by realizing that the summation in Eq. (26) may also be taken over all segment types except  $A$  and by using  $\sum_{B \neq A} \Lambda_B = \sum_B \Lambda_B - \Lambda_A$ . We then obtain for the slow-mode transport coefficients,

$$L_{AA}^s = \frac{\Lambda_A^2}{\sum_C \Lambda_C} - \Lambda_A, \quad (\text{A2a})$$

$$L_{AB}^s = \frac{\Lambda_A \Lambda_B}{\sum_C \Lambda_C}, \quad (\text{A2b})$$

so that Onsager's reciprocal relations are obeyed.

Before we rewrite the fast-mode flux of Eq. (28) we may first add the term  $\Lambda_A \sum_B \phi_B \nabla \mu_B$ . This term equals 0 according to Gibbs-Duhem relation  $\sum_B \phi_B d\mu_B = 0$ . Rewriting the extended Eq. (28) in the form of Eq. (A1) yields for the fast-mode transport coefficients,

$$L_{AA}^f = \Lambda_A (2\phi_A - 1), \quad (\text{A3a})$$

$$L_{AB}^f = \phi_A \Lambda_B + \phi_B \Lambda_A, \quad (\text{A3b})$$

so that again Onsager's reciprocal relations are obeyed.

#### APPENDIX B: DERIVATION OF EQUATION (42)

For a three-component system with  $N_A = N_B$  and  $B_A = B_B = B_C$ , we have a set of two independent fluxes, which may be written by the help of Eqs. (34) and either Eq. (37) or Eq. (38) as

$$J_A = -a \nabla \phi_A + b \phi_A \nabla (\phi_A + \phi_B), \quad (\text{B1})$$

$$J_B = -a \nabla \phi_B + b \phi_B \nabla (\phi_A + \phi_B) \quad (\text{B2})$$

where  $a = BkT/N_A$  and  $b = BkT(1/N_A - 1/N_C)$ . We want to solve this set for  $\phi_A(z)$  and  $\phi_B(z)$  with  $0 \leq \phi_A(z) + \phi_B(z) \leq 1$  for  $z \in [0, M+1]$ . The values for  $\phi_A(0)$ ,  $\phi_B(0)$ ,  $\phi_A(M+1)$ , and  $\phi_B(M+1)$  are known.

Summation of the differential equations and defining  $\phi_A(z) + \phi_B(z) = h(z)$ , we find for  $h(z)$ ,

$$h(z) = \frac{a}{b} \pm \frac{1}{b} \sqrt{a^2 + 2b(k_4 - J_C z)}. \quad (\text{B3})$$

The integration constant  $k_4$  and the flux  $J_C = -(J_A + J_B)$  can be calculated from  $h(0)$  and  $h(M+1)$ .  $h(z)$  must be positive and for our specific case ( $N_A > N_C$ ) we have  $a > 0$  and  $b < 0$ . Therefore, we must select the minus sign in Eq. (B3).

Using  $h(z)$ , we can now solve  $\phi_A(z)$  from Eq. (B1) by the standard procedures of separation of variables and variation of parameters. This introduces a new constant  $k_5$ .  $k_5$  and  $J_A$  may be calculated from  $\phi_A$  in  $z=0$  and  $z=M+1$ .  $J_B$  is then known from the values for  $J_C$  and  $J_A$ .  $\phi_B(z)$  is simply the difference between  $h(z)$  and  $\phi_A(z)$ , and  $\phi_C(z) = 1 - h(z)$ .

- [1] S.M. Engels and F.A.M. Leermakers, J. Chem. Phys. **114**, 4267 (2001).  
 [2] E.P.K. Currie *et al.*, Macromolecules **32**, 9041 (1999).  
 [3] F.A.M. Leermakers and J.M.H.M. Scheutjens, J. Phys. Chem.

**93**, 7417 (1989).

- [4] G.T. Pickett and A.C. Balazs, Langmuir **17**, 5111 (2001).  
 [5] J.M.H.M. Scheutjens and G.J. Fleer, J. Phys. Chem. **83**, 1619 (1979).

- [6] J.M.H.M. Scheutjens and G.J. Fleer, *J. Phys. Chem.* **84**, 178 (1980).
- [7] J. van Male, M.Sc thesis, Wageningen University, 1995.
- [8] E. Reister, M. Müller, and K. Binder, *Phys. Rev. E* **64**, 041804 (2001).
- [9] J.G.E.M. Fraaije, *J. Chem. Phys.* **99**, 9202 (1993).
- [10] J.G.E.M. Fraaije *et al.*, *J. Chem. Phys.* **106**, 4260 (1997).
- [11] R. Hasegawa and M. Doi, *Macromolecules* **30**, 3086 (1997).
- [12] C. Yeung and A.-C. Shi, *Macromolecules* **32**, 3637 (1999).
- [13] L.J.D. Frink, A. Thompson, and A.G. Salinger, *J. Chem. Phys.* **112**, 7564 (2000).
- [14] G.H. Fredrickson, V. Ganesan, and F. Drolet, *Macromolecules* **35**, 16 (2002).
- [15] F. Brochard, J. Jouffroy, and P. Levinson, *Macromolecules* **16**, 1638 (1983).
- [16] E.J. Kramer, P. Green, and C.J. Palmström, *Polymer* **25**, 473 (1984).
- [17] H. Sillescu, *Makromol. Chem., Rapid Commun.* **5**, 519 (1984).
- [18] F. Brochard and P.G. de Gennes, *Europhys. Lett.* **1**, 221 (1986).
- [19] G. Foley and C. Cohen, *J. Polym. Sci., Part B: Polym. Phys.* **25**, 2027 (1987).
- [20] W. Jilge *et al.*, *Macromolecules* **23**, 5001 (1990).
- [21] M.G. Brereton, *Prog. Colloid Polym. Sci.* **91**, 8 (1993).
- [22] E. Jabbari and N. Peppas, *Polymer* **36**, 575 (1995).
- [23] A.Z. Akcasu, *Macromol. Theory Simul.* **6**, 679 (1997).
- [24] I.Y. Erukhimovich and Y.V. Kudryavtsev, *Macromol. Theory Simul.* **8**, 247 (1999).
- [25] E. Pardo, J.P. Tomba, and J.M. Carella, *Comput. Theor. Polym. Sci.* **10**, 523 (2000).
- [26] P.F. Green and B.L. Doyle, *Macromolecules* **20**, 2471 (1987).
- [27] R.J. Composto, E.J. Kramer, and D.M. White, *Macromolecules* **21**, 2580 (1988).
- [28] T.E. Shearmur *et al.*, *Macromolecules* **29**, 7269 (1996).
- [29] T.E. Shearmur *et al.*, *Phys. Rev. E* **55**, R3840 (1997).
- [30] T.E. Shearmur *et al.*, *Polymer* **39**, 2155 (1998).
- [31] M. Geoghegan *et al.*, *Polymer* **40**, 2323 (1999).
- [32] H. Qiu and M. Bousmina, *Macromolecules* **33**, 6588 (2000).
- [33] P.R. Rouse, *J. Chem. Phys.* **21**, 1272 (1953).
- [34] P.G. de Gennes, *J. Chem. Phys.* **55**, 572 (1971).
- [35] M. Doi and S.F. Edwards, *The Theory of Polymer Dynamics* (Clarendon Press, Oxford, 1986).
- [36] M.G. Brereton *et al.*, *J. Chem. Phys.* **86**, 5174 (1987).
- [37] P.F. Green *et al.*, *Macromolecules* **18**, 501 (1985).
- [38] A.Z. Akcasu, G. Nägele, and R. Klein, *Macromolecules* **28**, 6680 (1995).
- [39] G.J. Fleer, J.M.H.M. Scheutjens, M.A. Cohen Stuart, T. Cosgrove, and B. Vincent, *Polymers at Interfaces* (Chapman & Hall, London, 1993).
- [40] H. Morita, T. Kawakatsu, and M. Doi, *Macromolecules* **34**, 8777 (2001).
- [41] O.A. Evers, J.M.H.M. Scheutjens, and G.J. Fleer, *Macromolecules* **23**, 5221 (1990).
- [42] P.J. Flory, *Principles of Polymer Chemistry* (Cornell University Press, Ithaca, 1953).
- [43] N.M. Maurits and J.G.E.M. Fraaije, *J. Chem. Phys.* **107**, 5879 (1997).
- [44] R.M. Barrer, *Proc. Phys. Soc. London* **58**, 321 (1946).
- [45] J. Crank, *The Mathematics of Diffusion* (Oxford University Press, Oxford, 1967).
- [46] S. Chakraborty, D.B. Dingwell, and D.C. Rubie, *Geochim. Cosmochim. Acta* **59**, 255 (1995).
- [47] Y. Liang, F.M. Richter, and E.B. Watson, *Geochim. Cosmochim. Acta* **60**, 5021 (1996).
- [48] P.C. Tortorici and M.A. Dayananda, *Mater. Sci. Eng., A* **261**, 64 (1999).
- [49] K. MacEwan and D.G. Leaist, *J. Phys. Chem. B* **106**, 10296 (2002).
- [50] T. Nishiyama, *Phys. Earth Planet. Inter.* **107**, 33 (1998).